

## Letters

### Scanning Force Microscopy Study of Patterned Monolayers of Alkanethiols on Gold. Importance of Tip-Sample Contact Area in Interpreting Force Modulation and Friction Force Microscopy Images

G. Bar\*

*Freiburger Materialforschungszentrum, Albert-Ludwigs Universität, Stefan-Meier-Strasse 21,  
D-79104 Freiburg, Germany*

S. Rubin, A. N. Parikh, B. I. Swanson, and T. A. Zawodzinski, Jr.

*Los Alamos National Laboratory, Los Alamos, New Mexico 87545*

M.-H. Whangbo

*Department of Chemistry, North Carolina State University,  
Raleigh, North Carolina 27695-8204*

*Received September 27, 1996. In Final Form: November 20, 1996*<sup>®</sup>

Several patterned monolayers of alkanethiols  $\text{CH}_3(\text{CH}_2)_{n-1}\text{SH}$  on a polycrystalline Au substrate were prepared by using microcontact printing and solution deposition methods, and their surfaces were examined by IR spectroscopy, scanning force microscopy, lateral force microscopy (LFM), and force modulation microscopy (FMM). Our work shows that LFM and FMM can detect differences in packing density of chemically identical molecules which are too small to be detected by IR, ellipsometry, and wetting measurements and suggests that the tip-sample contact area is an important parameter governing the contrasts of LFM and FMM images. Stiffness images obtained with FMM depend on changes in the Young's modulus of a sample surface as well as in the tip-sample contact area. As a result, a surface region of small modulus can have a large stiffness due to its large contact area.

#### Introduction

In recent years, thin organic films such as polymer films, Langmuir-Blodgett (LB) films, and self-assembled monolayers (SAMs) have been the subject of numerous scanning force microscopy (SFM) studies.<sup>1-8</sup> Different domains of phase-separated LB films prepared on a Si substrate are

detected in friction images obtained by lateral force microscopy (LFM) and stiffness images obtained by force

(3) Chi, L. F.; Anders, M.; Fuchs, H.; Johnston, R. R.; Ringsdorf, H. *Science* **1993**, *259*, 213.

(4) Overney, R. M.; Meyer, E.; Frommer, J.; Güntherodt, H.-J.; Fujihira, M.; Takano, H.; Gotoh, Y. *Langmuir* **1994**, *10*, 1281.

(5) Green, J.-B. D.; McDermott, M. T.; Porter, M. D.; Siperko, L. M. *J. Phys. Chem.* **1995**, *99*, 10960.

(6) Frisbie, C. D.; Rozsnyai, L. F.; Noy, A.; Wrighton, M. S.; Lieber, C. M. *Science* **1994**, *263*, 2071.

(7) Akari, S.; Horn, D.; Keller, H.; Schrepp, W. *Adv. Mater.* **1995**, *7*, 549.

(8) Wilbur, J. L.; Biebuyck, H. A.; MacDonald, J. C.; Whitesides, G. M. *Langmuir* **1995**, *11*, 825.

\* Author to whom all correspondence should be addressed.

<sup>®</sup> Abstract published in *Advance ACS Abstracts*, January 1, 1997.

(1) Binnig, G.; Quate, C. F.; Gerber, C. *Phys. Rev. Lett.* **1986**, *56*, 930.

(2) For a review on LB films and SAMs, see: Ulman, A., Ed. *An Introduction to Ultrathin Organic Films from Langmuir-Blodgett to Self-Assembly*; Academic Press: San Diego, CA, 1991.

modulation microscopy (FMM).<sup>3,4</sup> Different regions of patterned SAMs prepared on a polycrystalline Au substrate are also clearly distinguished in LFM and FMM images.<sup>6–8</sup> In order to correlate LFM and FMM images and to extract useful information from them, it is critical to know what factors govern image contrasts in LFM and FMM. This understanding is also necessary for correct interpretations of image contrast observed for polymers and so-called chemical force microscopy.<sup>6,7</sup> In the present work, we probe this question by preparing several patterned SAMs of alkanethiols  $\text{CH}_3(\text{CH}_2)_{n-1}\text{SH}$  on a polycrystalline Au substrate and characterizing their surfaces in terms of LFM, FMM, ellipsometry, contact angle measurements, and external reflection infrared (IR) spectroscopy.

### Theoretical Considerations

SFM height images and LFM friction images are simultaneously recorded in the contact mode SFM.<sup>9</sup> Height and friction images are respectively related to the vertical and lateral forces acting on the tip during scanning.<sup>9</sup> When the tip–sample repulsive interaction is negligible, height images of a sample are well described by the total electron density plot of the sample surface.<sup>10</sup> To interpret friction images of LFM, it is necessary to consider how the frictional (i.e., lateral) force  $F_f$  is related to the tip–sample contact area  $A$ . Surface forces apparatus experiments with contacting mica surfaces having either contaminant or liquid layers between them show<sup>11</sup> that in the absence of wear  $F_f$  is directly proportional to  $A$

$$F_f = \tau A \quad (1)$$

where  $\tau$  is the shear strength. This relationship is expected to be valid for our experiments as well, since they were carried out either in air or under water (see below).

In FMM the probe is oscillated vertically at a certain frequency with the tip in contact with the sample surface, and the force on the sample is modulated about a set-point force such that the average force on the sample is equivalent to that in simple contact mode SFM. The elastic deformation associated with the tip–sample contact can be estimated by Hertz theory.<sup>12</sup> Provided that a spherical tip of radius  $R$  and a plane surface under load  $P$  leads to a circular contact area  $A$  of radius  $a$  and an indentation depth  $x$ , the surface stiffness  $S$  is expressed as<sup>13</sup>

$$S = \partial P / \partial x = \epsilon a E^* \quad (2)$$

where  $\epsilon$  is a number between 1.9 and 2.4.<sup>14</sup>  $E^*$  is the effective modulus defined by  $1/E^* = (1 - n_1^2)/E_1 + (1 - n_2^2)/E_2$ , where  $E_1$  and  $E_2$  are Young's moduli and  $n_1$  and  $n_2$  are Poisson's ratios of the tip and sample. The stiffness defined by eq 2 is relevant for cases when the tip is in static contact with a sample surface. In FMM the tip–sample contact area varies with time throughout the duration of each oscillation. As described for the phase

imaging with tapping mode SFM,<sup>15</sup> therefore, it is necessary to use the time-averaged values of the contact area  $A$ , contact radius  $a$ , and stiffness  $S$  over one cycle of oscillation (i.e.,  $\langle A \rangle$ ,  $\langle a \rangle$ , and  $\langle S \rangle$ , respectively) in our description of stiffness images. Namely

$$\langle S \rangle = \epsilon \langle a \rangle E^* \propto \sqrt{\langle A \rangle} E^* \quad (3)$$

Equation 3 shows that the stiffness is proportional to  $E^*$ , which is dominated by the modulus of the sample when the tip is much harder than the sample (e.g.,  $E_1 \gg E_2$ ). Thus FMM provides a method of distinguishing surface features of different Young's moduli. However, the stiffness is also proportional to  $\langle A \rangle^{1/2}$ , and a softer material leads to a larger contact area  $A$ . Therefore, as found for the phase imaging of soft materials such as polymers,<sup>15</sup> the stiffness can be larger on a surface region of a smaller Young's modulus if the stiffness is dominated by the contact area.

### Experimental Section

Samples of patterned SAMs were prepared by a successive application of the microcontact printing ( $\mu\text{P}$ )<sup>16</sup> and solution deposition (SD) methods as previously described.<sup>17</sup> Briefly, the first component  $\text{CH}_3(\text{CH}_2)_{m-1}\text{SH}$  was transferred to a polycrystalline Au substrate by using a poly(dimethylsiloxane) stamp (with patterns of circles 2.5  $\mu\text{m}$  in diameter) which was then rapidly immersed in a 1 mM ethanolic solution of the second component,  $\text{CH}_3(\text{CH}_2)_{n-1}\text{SH}$ . Typical durations of  $\mu\text{P}$  and SD processes were 60 s and 10 min, respectively. This way, the final samples, consisting of circular features of  $-\text{S}(\text{CH}_2)_{m-1}\text{CH}_3$  moieties in the surrounding background of the second component  $-\text{S}(\text{CH}_2)_{n-1}\text{CH}_3$  are obtained. For convenience, the SAMs thus prepared will be referred to as  $Cm(\mu\text{P})/Cn(\text{SD})$ , where  $Cm$  and  $Cn$  refer to  $\text{CH}_3(\text{CH}_2)_{m-1}\text{S}$  and  $\text{CH}_3(\text{CH}_2)_{n-1}\text{S}$  groups, respectively. These samples were then investigated within a few hours of preparation by SFM, in air as well as under triply distilled water (TDW). The SFM images were obtained with a commercial microscope, Nanoscope III (Digital Instruments), while operating the instrument in contact and force modulation modes. We used commercial Si cantilevers with nominal force constants 0.02–0.7 N/m, the tips of which have a nominal radius of curvature 5–10 nm. Topography images were recorded in conventional height imaging mode, and the friction maps were recorded in the LFM mode.<sup>9</sup> For FMM measurements we used a modulation frequency around 8 kHz. Companion samples prepared simultaneously on larger substrates ( $2 \times 3 \text{ cm}^2$ ) were examined for structural characterization using ellipsometry, contact angle, and IR measurements. As representative examples, we describe our results obtained for C18( $\mu\text{P}$ )/C7(SD) and C18( $\mu\text{P}$ )/C18(SD) systems.

### Results and Discussion

The surfaces of the circular and surrounding regions of  $Cm(\mu\text{P})/Cn(\text{SD})$  are chemically identical, i.e., they are terminated with normal alkyl groups. Thus differences between the two regions detected by SFM are related most likely to differences other than chemical properties. A typical height image of C18( $\mu\text{P}$ )/C7(SD) recorded with SFM is presented in Figure 1a. The C18( $\mu\text{P}$ ) regions covered with C18 groups are higher, and hence brighter in the height SFM image, than the C7(SD) region covered with C7's. A typical friction image of C18( $\mu\text{P}$ )/C7(SD) recorded with LFM is shown in Figure 1b. The C18( $\mu\text{P}$ ) regions are darker than the C7(SD) region; i.e., the tip–surface

(9) Marti, O.; Colchero, J.; Mlynek, J. *Nanotechnology* **1990**, *1*, 141.  
(10) Magonov, S. N.; Whangbo, M.-H. *Surface Analysis with STM and AFM*; VCH: Weinheim, 1996.

(11) (a) Homola, A. M.; Israelachvili, J. N.; Gee, M. L.; McGuigan, P. M. *Trans. ASME: J. Tribol.* **1989**, *111*, 675. (b) Carpick, R. W.; Agrait, N.; Ogletree, D. F.; Salmeron, M. *J. Vac. Sci. Technol. B* **1996**, *14*, 1289.

(12) (a) Hertz, H. *J. Reine Angew. Math.* **1882**, *92*, 156. (b) Burnham, N. A.; Colton, R. J. In *Scanning Tunneling Microscopy and Spectroscopy*; Bonnell, D. A., Ed.; VCH: New York, 1993; Chapter 7.

(13) Pethica, J. B.; Oliver, W. C. *Phys. Scr.* **1987**, *T19*, 61.

(14) Kendall, K.; Tabor, D. *Proc. R. Soc. London, Ser. A* **1971**, *323*, 321.

(15) (a) Magonov, S. N.; Elings, V.; Whangbo, M.-H. *Surf. Sci. Lett.*, in press. (b) Whangbo, M.-H.; Magonov, S. N.; Bengel, H. *Probe Microsc.*, in press.

(16) Kumar, A.; Whitesides, G. M. *Appl. Phys. Lett.* **1993**, *63*, 2002.

(17) (a) Kumar, A.; Biebuyck, H. A.; Whitesides, G. M. *Langmuir* **1994**, *10*, 1498. (b) Bar, G.; Rubin, S.; Taylor, T. N.; Swanson, B. I.; Zawodzinski, A., Jr.; Chow, J. T.; Ferraris, J. P. *J. Vac. Sci. Technol. A* **1996**, *14*, 1794.

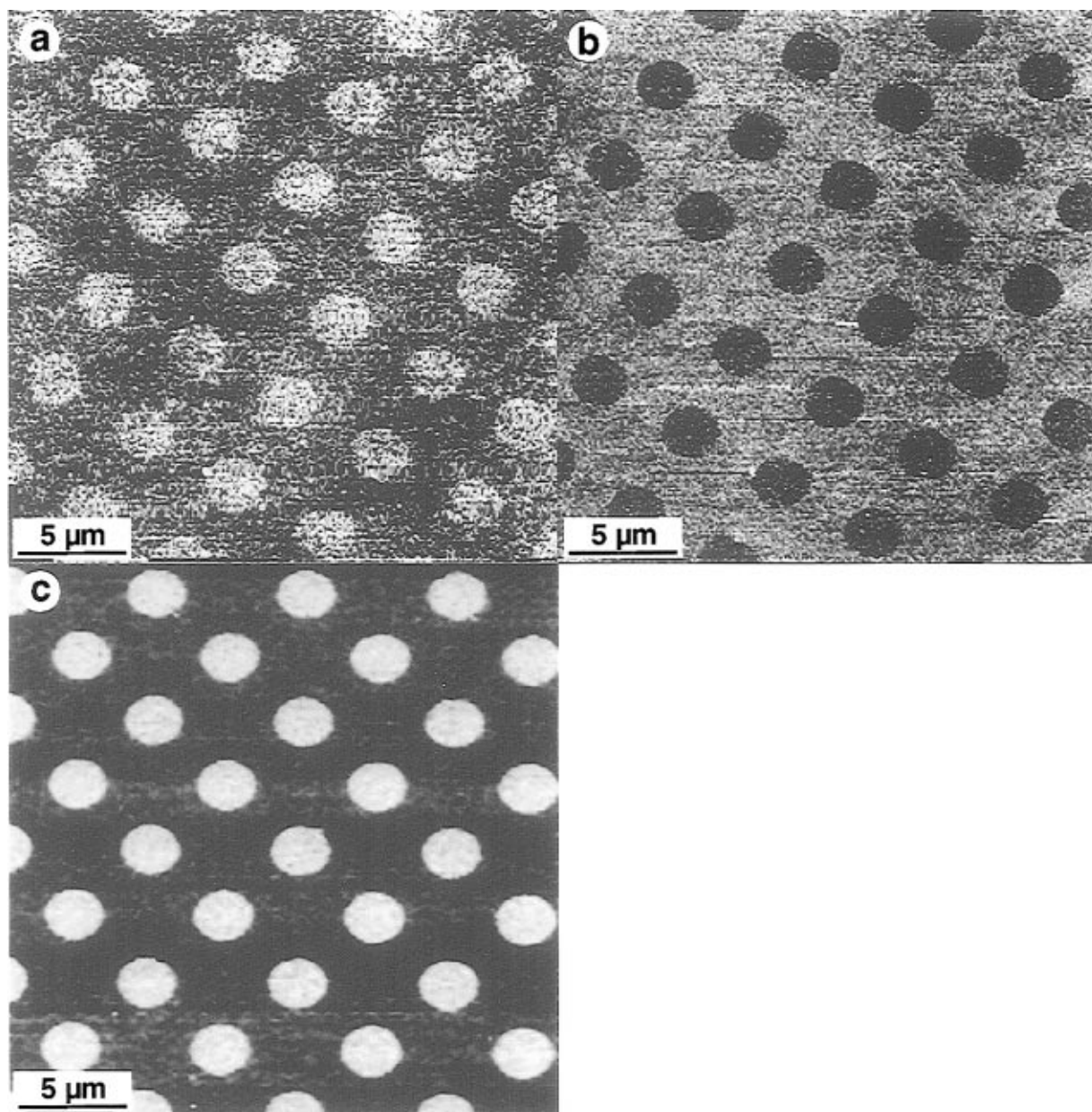


**Figure 1.** SFM images of C18( $\mu$ P)/C7(SD): (a) Height image recorded in air with a force of 17 nN. (b) Friction image recorded in air with a force of 17 nN. (c) Stiffness image recorded in air with a set-point amplitude of 1 mV. The image contrast covers height variations in the 10 nm range in (a), lateral deflection variations in the 0.3 V range in (b), and amplitude variations in the 5 nm range in (c).

friction is less on the C18( $\mu$ P) regions. IR investigations show that SAMs of short alkanethiols ( $m \leq 9$ ) are liquid-like<sup>18</sup> while long chain alkanethiols ( $m > 9$ ) form crystalline-like monolayers.<sup>19</sup> Thus, in agreement with the IR studies, the friction image of Figure 1b indicates that the contact area is smaller on the C18( $\mu$ P) surface than on the C7(SD) surface. This implies that the alkyl groups are more tightly packed on the C18( $\mu$ P) surface, which is reasonable because van der Waals attractions between alkyl groups are stronger between longer alkyl groups. A typical FMM image recorded for C18( $\mu$ P)/C7(SD) is presented in Figure 1c, where the C18( $\mu$ P) surface appears brighter. A brighter area of an FMM image is related to

a less stiff region of the surface.<sup>20</sup> Thus, the C18( $\mu$ P) surface is less stiff than the C7(SD) surface. From the viewpoint of Young's modulus alone, the C18( $\mu$ P) surface is expected to be stiffer, because our LFM measurements show that the alkyl groups are more tightly bound in the C18( $\mu$ P) surface than in the C7(SD) surface. However, the stiffness also depends on, and can be dominated by, the tip-sample contact area.<sup>15</sup> The image contrast of Figure 1c indicates that the more tightly packed area is less stiff because the contact area with the probe tip is much smaller there.

In SAMs of C18( $\mu$ P)/C18(SD) the circular and surrounding regions are both covered with C18 groups. To examine possible structural differences between the C18( $\mu$ P) and C18(SD) regions, we have investigated the

(18) Porter, M. D.; Bright, T. B.; Allara, D. L.; Chidsey, C. E. D. *J. Am. Chem. Soc.* **1987**, *109*, 3559.

(19) Reference 2, p 279 ff, and the references therein.

(20) We use the manufacturer's (Digital Instruments) contrast convention for the FMM images. Accordingly, a stiffer surface results in a higher deflection amplitude and is represented as a darker region in the FMM image.

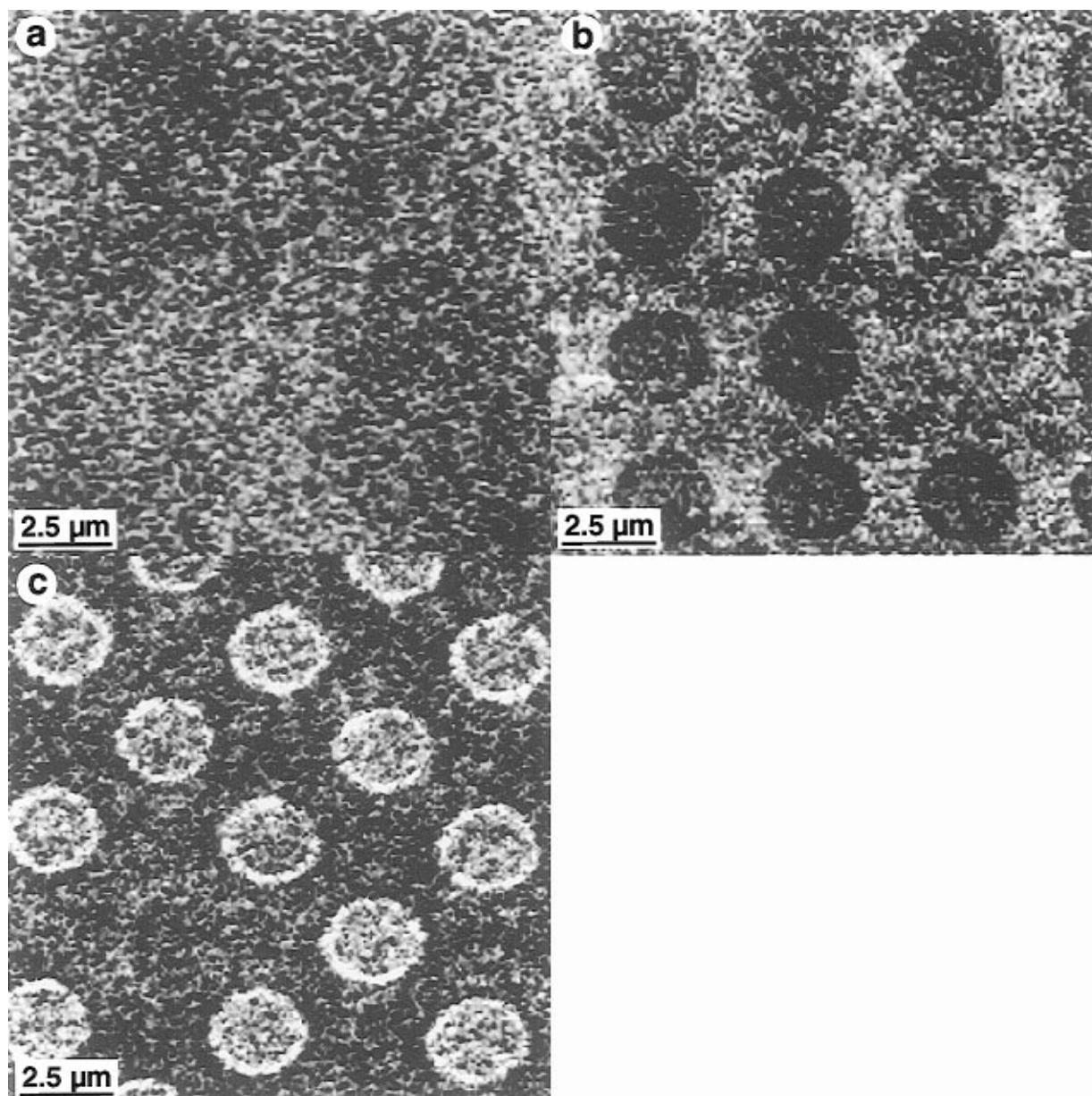


**Figure 2.** SFM images of C18( $\mu$ P)/C18(SD): (a) Height image recorded in triply distilled water with a force of 11 nN. (b) Friction image recorded in triply distilled water with a force of 11 nN. (c) Stiffness image recorded in air with a set-point amplitude of 100 mV. The image contrast covers height variations in the 5 nm range in (a), lateral deflection variations in the 0.3 V range in (b), and amplitude variations in the 0.5 nm range in (c).

average structural properties (e.g., film thickness, surface coverage, surface free energy, and chain-conformational order) using a set of companion samples and a control sample prepared by  $\mu$ P alone using a plain, featureless stamp. Ellipsometric film thicknesses estimated using null-ellipsometric data<sup>21</sup> obtained at 632.8 nm and 70° incidence gave a value of 20.5 ( $\pm 2$ ) Å for the C18( $\mu$ P)/C18(SD) samples. This value is indistinguishable within the experimental uncertainties from those reported previously for solution deposited octadecanethiol on gold monolayers.<sup>22</sup> Similarly, the evaluation of the critical surface tension as a measure of surface free energy ( $\gamma_c$ ) of the C18( $\mu$ P)/C18(SD) monolayer surface resulted in a value of  $\gamma_c = 21.0 \pm 0.5$  dyn cm<sup>-1</sup>. The latter measurement was done using contact angles of sessile drops of a series of liquid *n*-alkanes of known surface tensions from

*n*-decane to *n*-hexadecane according to the linear extrapolation method of Zisman.<sup>23</sup> The observed value of  $\gamma_c$  agrees quite well with that reported for a surface of methyl groups with near-limiting surface density<sup>24</sup> as well as with that reported previously for SD C18 monolayers. Estimates for the average chain-conformation and orientational order<sup>25</sup> in the C18( $\mu$ P)/C18(SD) samples were obtained using IR spectra. Spectral signature (spectra not shown) obtained in the C–H stretching region (2700–3100 cm<sup>-1</sup>) for C18( $\mu$ P)/C18(SD) samples were essentially indistinguishable from that obtained for the SD monolayer. A control sample prepared by  $\mu$ P alone using a featureless stamp also yielded identical spectral trace suggesting that any structural disparity between the samples is not

(21) Azzam, R. M.; Bashara, N. M. *Ellipsometry and Polarized Light*; North-Holland: Amsterdam, 1977.

(22) Laibinis, P. E.; Whitesides, G. M.; Allara, D. L.; Tao, Y.-T.; Parikh, A. N.; Nuzzo, R. G. *J. Am. Chem. Soc.* **1991**, *113*, 7152.

(23) Zisman, W. A. *Adv. Chem. Ser.* **1964**, No. 43, 1.

(24) Fox, H. W.; Zisman, W. A. *J. Colloid Sci.* **1952**, *7*, 428.

(25) Calculations of chain-orientational order from the C–H stretching region using a previously published procedure (Parikh, A. N.; Allara, D. L. *J. Chem. Phys.* **1992**, *96*, 927) resulted in identical values of chain-tilt = 24 ( $\pm 3$ )° and a chain-twist of 44° comparable to previously reported estimates (see, ref 22).

detectable by IR measurements. The positions of the conformation-sensitive peaks due to methylene C–H symmetric ( $d^+$ ) and antisymmetric ( $d^-$ ) stretching modes were valued at 2850.6 and 2919.2  $\text{cm}^{-1}$ , respectively. These values are well within the range of values reported for crystalline  $n$ -alkanes and densely packed, long-chain thiol monolayers.<sup>19</sup> Therefore, we conclude that all three classes of samples examined here are comprised of dominantly all-trans alkyl chains packed in a crystalline-like environment showing little differences in average molecular structure between them. The above measurements serve to show that in C18( $\mu$ P)/C18(SD) samples, the average structural properties fail to reflect any structural differences between the  $\mu$ P domains and the SD regions.

Since the difference between the C18( $\mu$ P) and C18(SD) regions is small, our SFM imaging of C18( $\mu$ P)/C18(SD) was recorded in triply distilled water to avoid any effects due to capillary forces and to minimize the total force interacting between the tip and sample. Nevertheless, we found identical results when experiments were conducted in air. The height image of C18( $\mu$ P)/C18(SD) (Figure 2a) shows no image contrast, because there is no height difference between the C18( $\mu$ P) and C18(SD) surfaces. The LFM image (Figure 2b) shows a clear contrast difference between the C18( $\mu$ P) and C18(SD) surfaces. The friction is lower on the C18( $\mu$ P) than on the C18(SD) surface, so that the tip–sample contact area is smaller on the C18( $\mu$ P) surface. Figure 2c presents a typical stiffness image recorded for C18( $\mu$ P)/C18(SD) with FMM in air. The C18( $\mu$ P) surface is brighter and is hence less stiff than the C18(SD) surface. Thus, the area showing the smaller contact area and lower friction as determined by LFM imaging is less stiff in FMM imaging, as found for C18( $\mu$ P)/C7(SD). Therefore, we speculate that the contrast difference between the C18( $\mu$ P) and C18(SD) surfaces of C18( $\mu$ P)/C18(SD) in the LFM and FMM imaging is most probably caused by a very small difference in the density of C18 groups on the two surfaces (with the alkyl groups more tightly packed on the C18( $\mu$ P) surface). Either the  $\mu$ P or  $\mu$ P/SD process must result in a higher density assembly of C18 groups on a Au substrate than does the SD process.<sup>26</sup>

Our discussion suggests that consideration of the tip–sample contact area is critical for understanding the contrast variations in LFM and FMM images. The contact area in LFM and FMM should increase with increasing the set-point force, and the rate of this increase should depend on the Young's modulus of the contact area.

(26) After a few minutes, the film thickness and contact angle are close to their limiting values (Bain, C. D.; Troughton, E. B.; Tao, Y.-T.; Ewall, J.; Whitesides, G. M.; Nuzzo, R. G. *J. Am. Chem. Soc.* **1987**, *109*, 3559). A more detailed study of the time dependence of the observed effects is in progress.

Therefore, we also examined how the LFM and FMM images of C18( $\mu$ P)/C7(SD) and C18( $\mu$ P)/C18(SD) depend on the set-point force. In the LFM images, the contrast difference between the C18( $\mu$ P) and C7(SD) regions is reversed as the set-point force increases beyond  $\sim 250$  nN, and that between C18( $\mu$ P) and C18(SD) disappears for the set-point force above  $\sim 60$  nN, and these changes are reversible. For the FMM images, however, the relative contrast remains the same but is often enhanced as the set-point force is varied from a very small value (15 nN) up to 300 nN. Furthermore, the image contrast observed in FMM was reproducible starting from a very small oscillating amplitude (e.g., 1 mV). A more detailed description of these results will be presented elsewhere.

### Concluding Remarks

Our work demonstrates that LFM and FMM are a sensitive method of surface analysis. Possible differences in packing density of chemically identical molecules, too small to be detectable by IR spectroscopy, can be easily distinguished in LFM and FMM images. For patterned SAMs composed of chemically different components, different packing densities can occur in chemically different regions. Then the contrasts of their LFM and FMM images will be determined not only by differences in tip interactions with chemically different surface regions but also by those in the packing densities of the different regions. Our work also suggests that the tip–sample contact area is an important parameter governing the contrasts of LFM and FMM images. Stiffness images of FMM are determined by the variation of the Young's modulus on a sample surface and by that of the tip–sample contact area. The surface stiffness increases with increasing the effective modulus and with increasing the contact area  $A$ . Since a sample of smaller modulus leads to a larger contact area, the stiffness can become larger on a surface of smaller modulus than on a surface of larger modulus.

**Acknowledgment.** G.B. wishes to thank Deutsche Forschungsgemeinschaft and Los Alamos National Laboratory (LANL) for financial support. Work at LANL was supported by the Office of Basic Sciences, Division of Materials Sciences, U.S. Department of Energy, and also by LANL Chemistry LDRD Funding. G.B. wishes to thank Dr. S. N. Magonov (Digital Instruments, Inc.) for helpful discussions. Work at North Carolina State University was supported by the Office of Basic Energy Sciences, Division of Materials Sciences, U.S. Department of Energy, under Grant DE-FG05-86ER45259.

LA960935M